Au, Pb, Bi, and U M-subshell ionization by protons

N. V. de Castro Faria, F. L. Freire, Jr., A. G. de Pinho,* and E. F. da Silveira
Departamento de Física, Pontifícia Universidade Católica, Caixa Postal 38071, Rio de Janeiro, Rio de Janeiro 22452, Brazil
(Received 18 October 1982)

M-subshell ionization cross sections of Au, Pb, Bi, and U by proton bombardment were obtained over the projectile range 0.3—4.0 MeV. X rays were detected by Si(Li) spectroscopy. At least one characteristic radiative transition line for each M subshell was isolated and measured. Radiative and nonradiative branching ratios were taken from theoretical calculations of Bhalla and McGuire. Our total x-ray-production cross sections are compared with the measurements of other authors. Comparison of our scaled subshell ionization cross sections with calculations in the plane-wave Born approximation shows, in general, good agreement. Uncertainties in fluorescence yields and in super—Coster-Kronig coefficients can introduce great imprecision in some experimentally determined subshell ionization cross sections.

I. INTRODUCTION

During the last decade much progress has been made in the study of K- and L-shell vacancies produced in heavy elements by MeV-energy proton impact.[1] However, M-shell studies are very scarce[2–5] due to experimental difficulties. Resolution is not as great a problem as a first look at an M x-ray spectrum obtained with Si(Li) spectroscopy seems to show. Groups of lines, where one or two transitions dominate, are isolated and extraction of a line representative of each subshell is possible (Fig. 1).

The measurement of efficiencies at the energies of M x-rays of heavy elements (~ 3 keV) is, however, quite a delicate problem. For high energies, experimental techniques are mandatory. In the energy region below 5 keV the scarcity of resolved lines from radiative sources and the uncertainty in the proton cross sections for K or L x rays limit the accuracy of absolute efficiency measurements. The fact that at these energies the efficiency is essentially due to the exponential absorption of photons opens the possibility of using a simple theoretical curve combined with experimental data.

As in the case of L-subshell studies, the knowledge of relative radiative decay rates, fluorescence yields, and Coster-Kronig factors is another obstacle in calculating the ionization cross sections from the measured x-ray-production cross sections. Precise and systematic measurements of these parameters are still lacking, and the use of theoretical calculations of Bhalla[6] and McGuire[7] is practically the only open possibility.

M-subshell ionization cross sections in our region of interest have been calculated in the plane-wave Born approximation (PWBA).[8] Scaling of these values as a universal function for the $3s$, $3p$, and $3d$ subshells for different values of θ and η/θ^2 is available and can be compared with experimental results. An important aspect of these curves for the M_1 subshell is their double inflection that reflects the two nontrivial nodes of the $3s$ electron wave functions. For the L_1 case,[9,10] the correlation between the density node and the dominant impact parameter obtained from the approximate position of the observed plateau in the ionization cross sections versus energy curve is well known.

The present work reports the measurements of the M-subshell and total x-ray-production cross sections and the determination of the M-subshell ionization cross sections of Au, Pb, Bi, and U for proton energies between 0.3 and 4.0 MeV. All relevant features mentioned in this introduction are analyzed and discussed in the text.

II. EXPERIMENTAL PROCEDURES AND ANALYSIS OF DATA

Thin targets ($\sim 5\ \mu g/cm^2$) obtained by vacuum evaporation of Au, Pb, and Bi onto Formvar, and of U onto Al, were employed in the experiments to avoid the need of large corrections of self-absorption of the x rays. Beams of 0.3—4.0-MeV protons were produced at the Van de Graaff accelerator of our university. Currents were kept below 30 nA to avoid pileup effects.

The x rays were detected by a Si(Li) detector with a measured resolution of 188 eV at 6.4 keV. The detector was positioned at 90° with respect to the beam and aimed

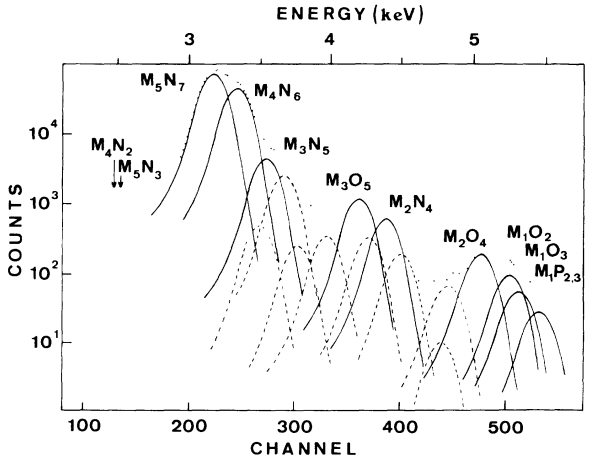

FIG. 1. M x-ray spectrum of U produced by 0.3-MeV protons. Also shown are the selected transition lines representative of each M subshell (solid curves), obtained after subtraction of the background and decomposition of the spectrum.

at the target by reflection. Its sensitive volume was separated from the target by a Mylar window 6 mm thick, air (17 mm), beryllium (25 μm), gold (200 Å), and a silicon dead layer (0.1 μm). In the case of a U target, a Kapton foil (80 μm) was introduced to eliminate the pileup of the Al K x rays with the $M\alpha\beta$ line of U.

The M x-ray intensities were normalized to the simultaneously detected $L\alpha$ x-ray lines from the same element avoiding, therefore, absolute measurements of the efficiency at low energies. In fact, precise measurements of the $L\alpha$ production cross sections are now available.[1,9–13] Relative efficiencies between 2 and 13 keV were obtained by three different methods, namely, the $K\alpha$ and $K\beta$ pairs of points, the K-shell relative production cross sections, and theoretical calculations.

The method of pairs of points employs the well determined ratio between $K\alpha$ and $K\beta$ lines.[14] Thin targets of elements with K x rays in the region of interest were irradiated with protons of 2 MeV and the radiation detected in the same geometry as the actual experiments.[10] This technique is more useful when the $K\alpha$ or $K\beta$ line of one element with atomic number Z falls between the $K\alpha$ and $K\beta$ lines of the element with $Z\pm1$, which happens for $Z\geq23$. In all cases the pair of points gives the derivative of the efficiency curve in the corresponding K x-ray energy. Below about 3 keV, the method used was to irradiate with protons very thin films prepared with two different elements, one having K x rays in the very low-energy region and the other higher than about 6 keV. For example, we prepared a target by evaporating copper (1 μg/cm^2) onto Formvar backing and aluminum (1 μg/cm^2) onto the copper surface. The number of atoms was determined by detecting the protons elastically scattered at 90° with respect to the beam direction and the x ray simultaneously. The relative K x-ray-production cross sections were taken from Ref. 15. Finally, the shape of the efficiency curve was obtained from theoretical calculations, with the thicknesses of the different absorption materials left as free parameters. The best fit to the experimental sets of points and derivatives changes very little the nominal values of the Mylar and Kapton thicknesses, and it is not very sensitive to small changes in the thickness of the other absorption materials. We estimated the uncertainties of the overall efficiency factor, that is, the relative efficiency for our experimental setup, as being less than 10%.

It can be seen in Fig. 1 that we have three well-defined groups of lines, the first dominated by the M_4N_6 and M_5N_7 transitions, the second by the M_3O_5 and M_2N_4 ones, and the third by the M_2O_4 line and the complex cluster of lines $M_1O_{2,3}$ and $M_1P_{2,3}$. This fact greatly simplifies the analysis of spectra and any method based on realistic peak profiles can be used to extract unique and accurate values for the intensities of the lines. The graphical method employed is the same that was used in Refs. 9 and 10, which essentially consists in the following three steps. In the first one, peak profiles were obtained for different regions of the spectra from $K\alpha$ lines of some elements (e.g., Cl and Sc). In the second step, we use the well-known energy of the lines, the theoretical values of the branching ratios[6] of each subgroup M_i ($i=1-5$), modified by detection efficiency, and the peak profiles to build up each subgroup. Finally, the subgroups were assembled together and their relative intensities changed to fit the experimental spectrum without background. For

TABLE I. X-ray-production cross sections (in barns) of selected lines representative of gold M subshells. Estimates of total absolute uncertainties are ±15% for M_1 and M_2 lines, ±13% for M_3 lines, and ±11% for M_4 and M_5 lines.

Energy (MeV)	M_5N_7	M_4N_6	M_3O_5	M_2N_4	$M_1O_{2,3}+M_1P_{2,3}$
0.3	69.9	37.3	0.21	0.25	0.024
0.4	117.6	77.3	0.46	0.52	0.051
0.5	196.0	126.9	0.91	1.04	0.067
0.6	240.6	157.6	1.44	1.52	0.12
0.7	273.9	179.5	1.78	2.00	0.17
0.8	370.2	209.6	2.55	3.27	0.26
0.9	471.9	193.6	3.20	3.27	0.41
1.0	418.9	309.2	4.35	4.88	0.50
1.2	533.5	341.2	5.01	6.02	0.57
1.4	622.6	369.9	5.40	8.52	0.63
1.6	648.7	508.6	7.21	11.3	0.82
1.8	729.5	600.3	8.57	14.1	1.18
2.0	714.4	710.4	9.46	13.9	1.31
2.2	711.6	763.8	9.95	16.0	1.48
2.4	707.9	778.7	11.49	16.8	1.70
2.6	884.8	766.3	11.56	17.2	1.72
2.8	864.9	775.9	11.24	17.4	1.74
3.0	924.0	875.4	13.00	23.1	1.66
3.2	1021.0	848.0			
3.4	1027.0	845.5			
3.6	1063.7	861.2			
3.8	1037.7	853.9			
4.0	1042.1	874.3			

TABLE II. Same as for Table I, for lead.

Energy (MeV)	M_5N_7	M_4N_6	M_3N_5	M_3O_5	M_2N_4	$M_1O_{2,3}+M_1P_{2,3}$
0.3	45.5	18.7	1.66	0.14	0.14	0.022
0.4	82.4	37.5	3.72	0.32	0.30	0.035
0.5	129.8	57.2	7.83	0.67	0.55	0.059
0.6	168.2	72.5	12.3	1.08	0.83	0.098
0.7	208.1	93.6	17.9	1.56	1.20	0.14
0.8	264.9	130.0	28.7	2.51	1.92	0.21
0.9	270.9	134.6	29.9	2.57	1.99	0.24
1.0	346.2	170.1	44.8	3.83	2.81	0.37
1.2	414.7	198.8	61.3	5.33	4.08	
1.4	503.1	257.3	85.5	7.23	5.08	
1.6	583.8	282.4	110.4	9.57	6.68	
1.8	627.6	315.6	126.4			
2.0	708.9	386.1	163.8			
2.2	728.6	442.6	173.0			
2.4	782.2	465.8	193.6			
2.6	879.2	562.1	219.8			
2.8	845.7	549.3	204.7			
3.0	935.8	563.6	210.2			
3.2	904.1	575.8	218.2			
3.4	903.7	580.1	227.6			
3.6	895.7	568.2	224.9			
3.8	880.7	563.1	206.8			
4.0	856.9	556.6	208.3			

the determination of the M_4- and M_5-subshell ionization cross sections the lines of the first group, i.e., M_4N_6 and M_5N_7, could be selected and extracted with good precision in all the cases. The same thing occurred for the M_3 subshell with the M_3O_5 transition, a line of the second group. For energies smaller than 1 MeV, M_1 and M_2 subshells were analyzed from the lines $M_1O_{2,3}$,$M_1P_{2,3}$ and M_2O_4 of the third group. For higher energies, background coming from bremsstrahlung prevents the use of the lines of this group. We can still use the M_2N_4 line of the second group to get information about the M_2 ionization cross section. We watched the background at all energies by constantly irradiating the target substrates.

III. RESULTS AND DISCUSSION

In Tables I—IV we present the experimental x-ray-production cross sections of the selected lines representative of each M subshell, i.e., the areas of the M lines normalized to the $L\alpha$ intensities and corrected for the $L\alpha$ production cross sections and the global relative efficiency factor. All angular distributions of L and M x rays were

TABLE III. Same as for Table I, for bismuth.

Energy (MeV)	M_5N_7	M_4N_6	M_3O_5	M_2N_4	$M_1O_{2,3}+M_1P_{2,3}$
0.3	46.9	12.2	0.17	0.17	0.021
0.4	69.4	35.4	0.30	0.33	0.030
0.5	118.3	58.7	0.69	0.55	0.048
0.6	154.5	78.9	0.97	0.95	0.067
0.7	202.4	100.8	1.71	1.43	0.11
0.8	243.5	92.9	2.16	2.09	0.18
0.9	295.7	158.4	2.91	2.62	0.27
1.0	333.0	194.3	3.58	3.70	0.33
1.2	446.5	242.2	5.64	5.87	0.51
1.4	547.4	294.6	7.11	8.10	0.86
1.6	601.3	316.4	8.77	9.10	1.02
1.8	673.0	357.8	11.0	9.66	1.53
2.0	692.5	427.8	13.0	11.3	
2.2	735.6	482.7	12.5	14.2	
2.4	758.5	493.5	13.3	15.0	
2.6	781.2	524.7	13.8	15.5	
2.8	836.8	536.5	14.5	17.7	
3.0	824.3	531.2	12.7	18.2	

TABLE IV. Same as for Table I, for uranium.

Energy (MeV)	M_3N_7	M_4N_6	M_3O_5	M_2N_4	M_2O_4	$M_1O_{2,3}+M_1P_{2,3}$
0.3	19.7	10.2	0.61	0.068	0.019	0.014
0.4	30.2	15.8	1.04	0.10	0.029	0.019
0.5	56.9	31.3	2.18	0.19	0.054	0.046
0.6	80.7	44.0	3.48	0.35	0.10	0.049
0.7	94.3	53.6	4.86	0.43	0.12	0.061
0.8	111.9	63.4	6.55	0.52	0.18	0.083
0.9	128.8	73.5	8.66	0.69	0.20	0.090
1.0	144.0	79.2	10.0	0.99	0.28	0.13
1.2	181.3	100.3	13.6	1.45	0.36	
1.4	191.3	122.4	21.6	2.16		
1.6	218.3	146.6	28.9	2.57		
1.8	255.1	168.9	33.6	3.23		
2.0	311.2	191.0	38.9	3.93		
2.2	348.1	212.2	45.1	4.74		
2.4	359.7	228.8	48.4	5.78		
2.6	455.8	234.5	53.0	7.04		
2.8	495.6	257.1	56.7	8.97		
3.0	493.3	255.9	56.6	8.09		

assumed to be isotropic. We assign an absolute standard deviation ranging from 15% for the M_1 group of lines to 11% for the M_4N_6 and M_5N_7 lines. They come mainly from the relative efficiency corrections uncertainties. Other sources of errors were the uncertainties in the $L\alpha$ production cross sections, around 5%, and the relative accuracy of our graphical method of spectra analysis, which was not greater than 5%. The statistical errors from counting were, in most of the cases, negligible.

To compare our measurements with available data in the literature,[2–5] we calculated the total M x-ray cross sections with the values of Tables I–IV and the theoretical radiative branching ratios of Bhalla.[6] The cross sections are presented in Fig. 2 together with the results of other authors. In fact, the data from Refs. 2–5 were obtained taking average efficiencies for the first and second groups, the spectra not being decomposed into their components. When we use essentially the same technique for our data, we obtained results differing by no more than 5% from

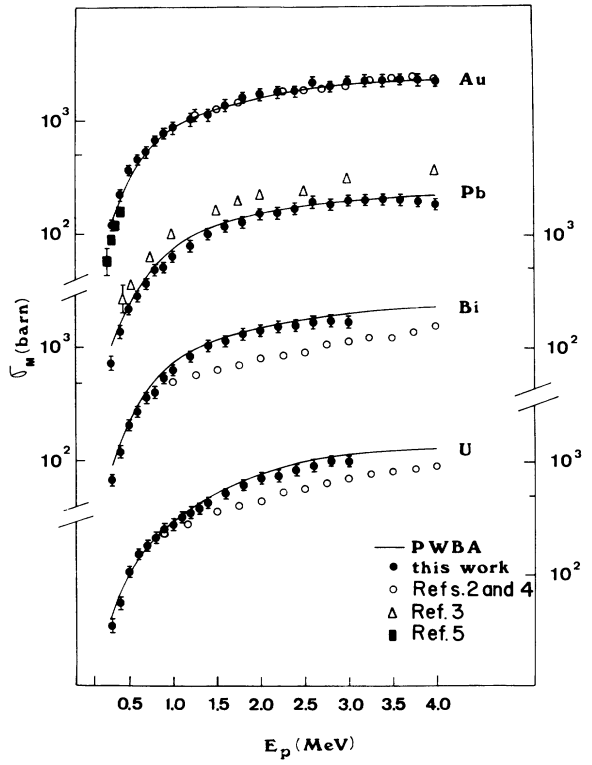

FIG. 2. Experimental total M x-ray-production cross sections for Au, Pb, Bi, and U. Also presented are PWBA theoretical curves.

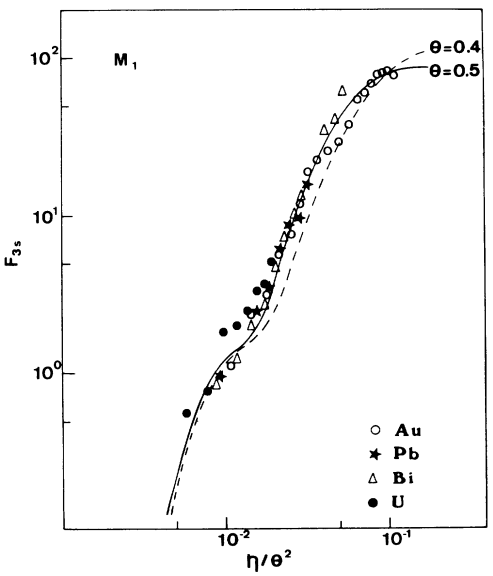

FIG. 3. Scaled experimental M_1 ionization cross sections for Au, Pb, Bi, and U. Also presented are PWBA theoretical curves for two different values of θ.

our experimental points represented in the figures. The solid lines are theoretical calculations of the total production cross sections obtained with the plane-wave Born-approximation total ionization cross sections[8] and average fluorescence coefficients defined in Ref. 7.

The ionization cross sections of each subshell, presented in Figs. 3–7, can be written as explicit functions of the x-ray-production cross sections:

$$\sigma_I^{M_1}=\left[\frac{1}{\omega_1}\right]\sigma_x^{M_1}, \tag{1}$$

$$\sigma_I^{M_2}=\left[\frac{1}{\omega_2}\right]\sigma_2^{M_2}-S_{12}\sigma_I^{M_1}, \tag{2}$$

$$\sigma_I^{M_3}=\left[\frac{1}{\omega_3}\right]\sigma_x^{M_3}-S_{23}\sigma_I^{M_2}-(S_{13}+S_{12}S_{23})\sigma_I^{M_1}, \tag{3}$$

$$\sigma_I^{M_4}=\left[\frac{1}{\omega_4}\right]\sigma_x^{M_4}-S_{34}\sigma_I^{M_3}-(S_{24}+S_{23}S_{34})\sigma_I^{M_2}-(S_{14}+S_{12}S_{24}+S_{13}S_{34}+S_{12}S_{23}S_{34})\sigma_I^{M_1}, \tag{4}$$

$$\sigma_I^{M_5}=\left[\frac{1}{\omega_5}\right]\sigma_x^{M_5}-f_{45}\sigma_I^{M_4}-(S_{35}+S_{34}f_{45})\sigma_I^{M_3}-(S_{25}+S_{23}S_{35}+S_{24}f_{45}+S_{23}S_{34}f_{45})\sigma_I^{M_2}$$
$$-(S_{15}+S_{12}S_{25}+S_{13}S_{35}+S_{14}f_{45}+S_{12}S_{23}S_{35}+S_{12}S_{24}f_{45}+S_{13}S_{34}f_{45}+S_{12}S_{23}S_{34}f_{45})\sigma_I^{M_1}, \tag{5}$$

where ω_i is the fluorescence yield of the i subshell, f_{ij} are the Coster-Kronig factors, and S_{ij} are the super–Coster-Kronig factors calculated by McGuire.[7] The relation between the x-ray-production cross sections $\sigma_x^{M_i}$ and the experimental transition cross sections σ_x^{κ} listed in Tables I–IV is

$$\sigma_x^{M_i}=\sigma_x^{\kappa}(\Gamma_i/\Gamma_i^{\kappa}), \tag{6}$$

where Γ_i is the total radiative width and Γ_i^{κ} is the partial radiative width for the κ transition of the i subshell.[6]

Calculations of M-subshell ionization were performed by Johnson *et al.*[8] with the plane-wave Born approximation and presented in the form of scaled ionization cross sections obtainable from the functions $F_{3l}(\eta/\theta^2,\theta)$, where l denotes the orbital angular momentum quantum number. The dimensionless parameters η and θ are the scaled incident energy and binding energy,[16,17] respectively.

Total M-shell ionization cross sections were also obtained by the same authors starting from the ionization cross section of each of the five energy eigenstates, summing them with coefficients reflecting the statistical weight of the $3s$, $3p$, and $3d$ electrons. Finally, with an average fluorescence coefficient,[7] we obtained the total M x-ray-production cross section. These cross-section calculations reproduce our results very well (Fig. 2), showing

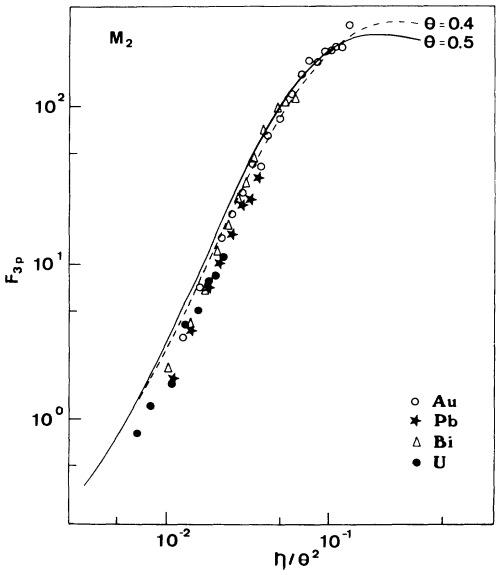

FIG. 4. Same as in Fig. 3, for M_2.

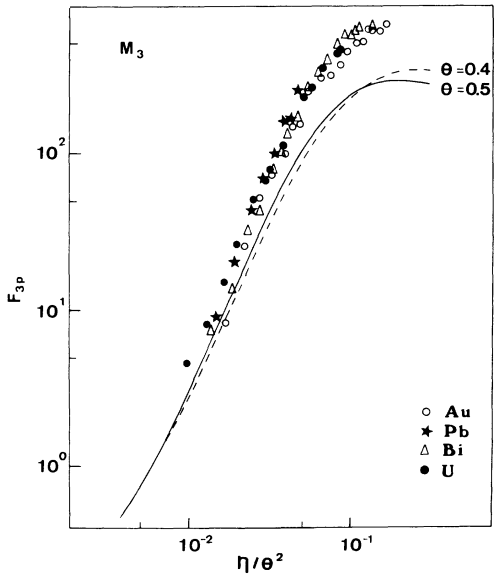

FIG. 5. Same as in Fig. 3, for M_3.

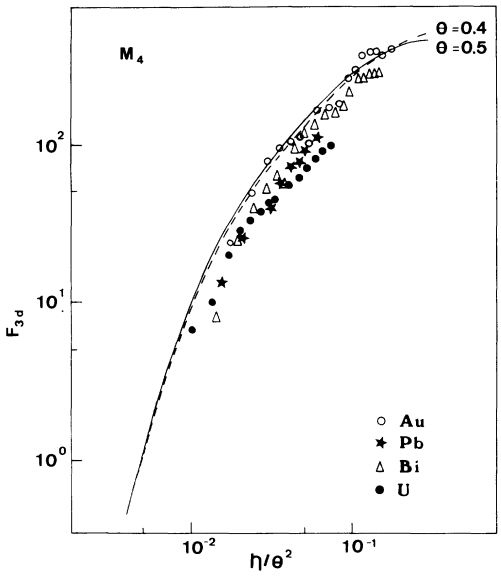

FIG. 6. Same as in Fig. 3, for M_4.

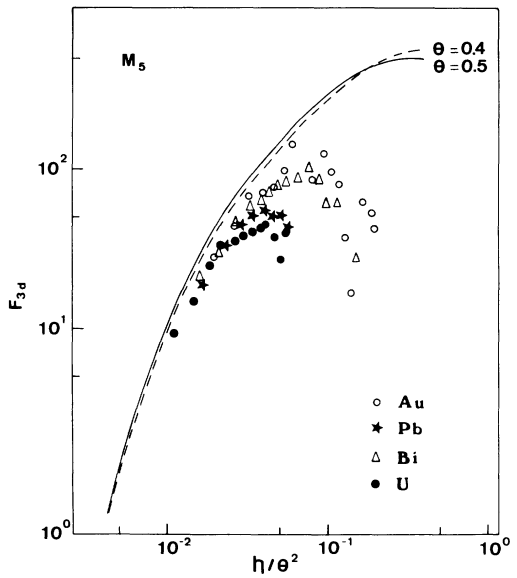

FIG. 7. Same as in Fig. 3, for M_5.

the coherence of the data, particularly of the dominant lines M_4N_6 and M_5N_7 which are influenced very little by the intensities of the transitions going to the M_1, M_2, and somewhat less, to the M_3 subshells.

The scaled ionization cross sections are presented in Figs. 3—7. The experimental points concerning the M_1 subshell exhibit very clearly the plateau corresponding to the inner node of the radial $3s$ wave function. To observe the outer node would require an impact energy too low for our accelerator. The inflection associated with the single nontrivial node of the $3p$ wave function is much less pronounced. Agreement with the theoretical calculations is very poor for M_3 and M_5 subshells despite the fact that the $M_1O_{2,3}$, $M_1P_{2,3}$, and M_2O_4 or M_2N_4 lines are more difficult to extract from the spectra than the M_3O_5 or M_5N_7 lines. With our data we are not able to give a definite explanation of this fact, but we can notice that a set of fluorescence yields and of super—Coster-Kronig factors can be found that makes the data agree well with the theoretical calculations in all the subshells. In fact, if we take the ratio between the ionization cross sections $\sigma_1^{M_3}/\sigma_1^{M_2}$ for experimental results and compare with the PWBA predictions one can observe that the ratio ω_3/ω_2 should be of the order of two, for all elements studied. Thus, if we multiply ω_3 by a factor of about 2 and if ω_2 is also modified and reduced about 20%, see Table V, our data come into good agreement with the theoretical curves, as is shown in Fig. 8.

IV. SUMMARY AND CONCLUSIONS

We have measured the total M-shell x-ray-production cross sections of Au, Pb, Bi, and U by proton impact in the energy range 0.3—4.0 MeV. We also have presented the five subshell ionization cross sections in the form of scaled cross sections that can be directly compared with the three universal functions $F_{3l}(n/\theta^2,\theta)$ of the plane-wave Born approximation.

As should be expected from the beginning, the PWBA

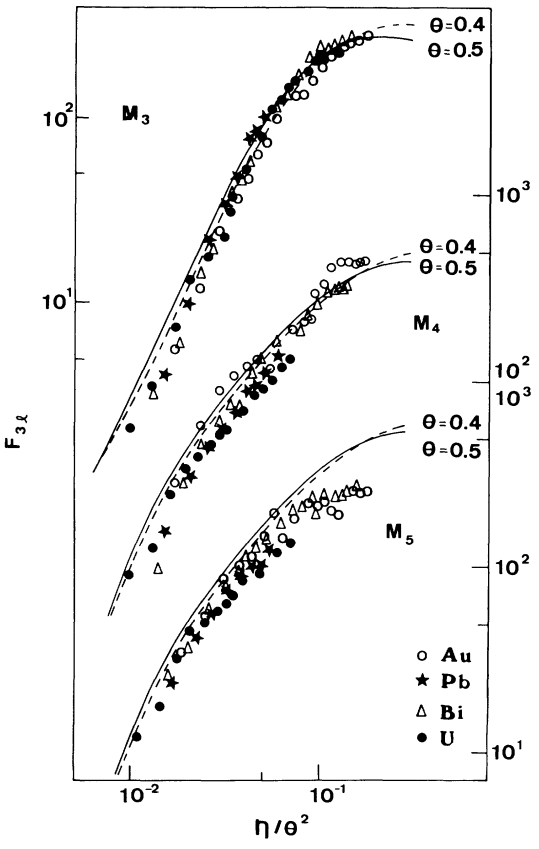

FIG. 8. Scaled experimental M_3, M_4, and M_5 ionization cross sections calculated with the modified ω_3 and ω_2. Also presented are PWBA theoretical curves for two different values of θ.

TABLE V. Fluorescence yield values.

Element	ω_2 $(10^{-3})^a$	ω_2 $(10^{-3})^b$	ω_3 $(10^{-3})^a$	ω_3 $(10^{-3})^b$
Au	4.23	3.30	4.20	8.40
Pb	5.90	4.80	5.02	10.1
Bi	6.52	5.80	5.33	11.0
U	16.2	13.0	9.00	18.5

[a]Calculated by McGuire, Ref. 7.
[b]Inferred from our results.

furnishes a very satisfactory description of the M-shell ionization by energetic massive projectiles. The PWBA is usually corrected for the following three effects[17]: the relativistic effects on the electron wave functions, the retardation and deflection of the projectile by the Coulomb field of the target nucleus, and the perturbation of the atomic states of the target by the projectile. However, it would be incorrect to impute to any of these effects the discrepancies we observed between some experimental data and the PWBA predictions. From the three above-mentioned effects only the last one, the binding effect, could be of some importance in the lower part of the region of energy that has been explored by us. The severe deviations from the PWBA results we observed mainly in the M_3 and M_5 cases are very probably due to our lack of knowledge of the exact values of the radiative and nonradiative partial widths. A particular problem seems to occur with the calculated[7] values of the fluorescence yields of the $3p$ subshells. So far as we know, there are no experimental data on M_2- and M_3-subshell yields. We observed that the modification in the distribution of the p-shell total radiative yield between M_2 and M_3 that seems to be necessary to improve the agreement of experiment and theory is a larger ω_3 and a lower ω_2 than calculated by McGuire.[7] More experimental information about the mechanisms of creation and filling of M-subshell vacancies is required before more detailed conclusions can be brought forward.

Note added in proof. After this paper was submitted for publication, a paper by R. Mehta, J. L. Duggan, J. I. Price, and F. D. McDaniel was published, Phys. Rev. A 26, 1883 (1982), which presents total M-shell x-ray-production cross sections in thin targets of Au, Pb, Bi, and U by 0.3—2.6-MeV protons. Their results are systematically smaller than ours. In the common energy interval the average difference is 30% for Au and 13% for Pb, Bi, and U. Moreover, their σ_M^x versus E curves are steeper than ours for Au and U, the contrary being observed for Pb and Bi. The more significant difference between the two papers is the way the overall detection efficiencies were considered.

ACKNOWLEDGMENTS

This research was supported in part by the Conselho Nacional de Pesquisa do Brasil and by the Financiadora de Estudos e Projetos.

*Present address: Institut de Physique Nucléaire de Lyon, F-69622 Villeurbanne, France.

[1]*Proceedings of the Second Workshop on Inner Shell Ionization by Light Atoms,* edited by H. Paul (North-Holland, Amsterdam, 1982) [special issue, Nucl. Instrum. Methods 192, (1982)].
[2]K. Ishii, S. Morita, H. Tawara, H. Kaji, and T. Shiokawa, Phys. Rev. A 11, 119 (1975).
[3]C. E. Busch, A. B. Baskin, P. H. Nettles, S. M. Shafroth, and A. W. Waltner, Phys. Rev. A 7, 1601 (1973).
[4]K. Sera, K. Ishii, A. Yamadera, A. Kuwako, M. Kamya, M. Sebata, S. Morita, and T. C. Chu, Phys. Rev. A 22, 2536 (1980).
[5]M. Sarkar, H. Mommsen, W. Sarter, and P. Schürkes, J. Phys. B 14, 3163 (1981).
[6]C. P. Bhalla, J. Phys. B 3, 916 (1970).
[7]E. J. McGuire, Phys. Rev. A 5, 1043 (1972).
[8]B. H. Choi, Phys. Rev. A 7, 2056 (1973); D. E. Johnson, G. Basbas, and F. D. McDaniel, At. Data Nucl. Data Tables 24, 1 (1979); IEEE Trans. Nucl. Sci. NS-26, 1162 (1979).
[9]C. V. Barros Leite, N. V. de Castro Faria, and A. G. de Pinho, Phys. Rev. A 15, 943 (1977).
[10]E. L. B. Justiniano, A. A. G. Nader, N. V. de Castro Faria, C. V. Barros Leite, and A. G. de Pinho, Phys. Rev. A 21, 73 (1980).
[11]R. C. Bearse, D. A. Close, J. J. Malanify, and C. J. Umbarger, Phys. Rev. A 7, 1269 (1973).
[12]D. Bhattacharya, S. K. Bhattacherjee, and S. K. Mitra, J. Phys. B 13, 967 (1980).
[13]W. Sarter, H. Mommsen, M. Sarkar, P. Schürkes, and A. Weller, J. Phys. B 14, 2843 (1981).
[14]S. I. Salem, S. L. Panossian, and R. A. Krause, At. Data Nucl. Data Tables 14, 91 (1974).
[15]S. A. E. Johansson and T. B. Johansson, Nucl. Instrum. Methods 137, 473 (1976).
[16]E. Merzbacher and H. W. Lewis, *Handbuch der Physik* (Springer, Berlin, 1958), Vol. 34, p. 166.
[17]G. Basbas, W. Brandt, and R. M. Laubert, Phys. Rev. A 7, 938 (1973).